



Shahrood University of
Technology



Iranian Society of
Mining Engineering
(IRSME)

Failure Mechanism of Rock Pillar Containing Two Edge Notches: Experimental Test and Numerical Simulation

Amir Rezaei, Vahab Sarfarazi*, Nima Babanouri, Mohamad Omidimanesh, and Shirin Jahanmiri

Department of Mining Engineering, Hamedan University of Technology, Hamedan, Iran

Article Info

Received 1 April 2023

Received in Revised form 12 April 2023

Accepted 18 April 2023

Published online 18 April 2023

DOI:10.22044/jme.2023.12909.2341

Keywords

Rock pillar

Edge notch

Experimental test

Particle flow code

Abstract

Non-persistent joints are geologic occurrences in rocks that weaken pillars because they are present within them. Using practical tests and numerical models, it has been determined how edge notches affect the way pillars break. Gypsum samples that are notched and have dimensions of 70 mm by 70 mm by 50 mm are created. Gypsum's Young modulus, Poisson ratio, compressive strength, and tensile strength are 5.5 GPa, 0.27, 8 MPa, and 1.1 MPa, respectively. 10-, 20-, and 30-degree notch angles are used. The model receives an axial stress at a rate of 0.05 mm/min. On a rock pillar, numerical simulation is carried out concurrently with an experimental test. The findings indicate that the joint angle is mostly responsible for the failure process. The fracture pattern and failure mechanism of the pillars are connected to the compressive strengths of the specimens. At the notch points, two significant splitting tensile fractures spread vertically until coalescing with the top and lower boundaries of the models. On the left and right sides of the pillar, two rock columns are also taken out. The overall number of cracks rises as sample loading increases. The model's deformation at the start of loading reflect a linear elastic behavior, and the number of fractures steadily grows. When the number of cracks increases, the curve becomes non-linear, and the force being applied peaks. When the sample can no longer tolerate the applied force, a dramatic stress decrease occurs. The macro-failure over the whole model is what leads to the greater stress decrease following the peak load. In actuality, the reduced stress reduction is accompanied by more overall fractures. Similar findings are shown in both the experimental testing and numerical modeling.

1. Introduction

Rock layers contain discontinuities that could pose support and stability issues both during and after mine development. In a rock mass, these discontinuities appear as distinct surfaces, where sliding action may or may not take place. Depending on how the discontinuity is oriented in relation to the direction of the tension, the strength of a rock sample with a discontinuity is considerably lower than the strength of a rock sample that is intact [1]. The behavior of pillars has been demonstrated to be comparable to that of a rock sample, indicating that the power of the pillar is also influenced by the discontinuity in the pillar (Figure 1).

Numerous rock engineering techniques have demonstrated that the start and spread of cracks in the rock bulk are the primary causes of rock

engineering disasters. Investigating the fracture evolution behavior of flawed rock in different rock engineering is, therefore, extremely important. Numerous academics have done experimental study on rock and rock-like materials with various fracture shapes to fully explore the failure mechanism of flawed rock [3-7]. Many laboratory studies on gypsum specimens with pre-existing fractures were carried out by Shen *et al.* According to their findings, differing fracture geometries led to noticeably diverse stress fields in the rock bridge region, which, in turn, led to a variety of failure mechanisms [9]. The effect of bridge inclination on the failure modes of rock-like materials with faults was studied by Mughieda and Alzo'ubi. They noticed that the concentration of tensile stress caused wing cracks to begin to spread prior to

✉ Corresponding author: vahab.sarfarazi@gmail.com (V. Sarfarazi)

collapse [10]. In laboratory testing, Cheng *et al.* investigated the coalesce behaviors of rock with numerous faults, and found that the failure process was comparable to that of a defective pair [10]. To evaluate the deformability and strength of a rock joint, Chiu *et al.* [12] suggested a rough-joint model, and investigated the properties of shear displacements, normal closure, and shear dilations of the joints. The compressive failure process of rock-like materials with X-type defects aligned in the loading direction was researched by Zhang *et al.* [13]. They demonstrated the fracture mechanisms and crack evolution laws of the rock mass with X-type flaws. The failure behavior of jointed rock masses with varying joint densities, and joint distributions was studied by Wang *et al.* [14]. In a series of static and dynamic compression experiments on jointed rock samples that had been filled with various filling materials, Chai *et al.* [15] were able to determine the strengths and failure mechanisms of the filled rock joints. Many numerical analytical techniques have been employed alongside experimental research to examine the failure behaviors of the rock mass [16–27]. The particle flow code (PFC), one of these numerical techniques, has been extensively developed to provide light on the failure process for rock by directly reproducing cracks by bonding fractures between particles [28]. Fakhimi *et al.* [29] numerically investigated the failure of sandstone with a circular defect under biaxial compression using PFC2D. They showed that the damaged regions seen in laboratory testing could be replicated by the PFC2D numerical model. By using PFC2D, Lee and Jeon [30] examined the fracture development of granite that had both horizontal and slope faults. Their findings demonstrated that the PFC2D modeling and the laboratory test results had a respectable level of agreement. By the PFC3D modeling and practical test, Khazaei *et al.* [31] studied the deterioration process of intact rocks based on the acoustic emission energies. During uniaxial compression, Jin *et al.* [32] used PFC2D to examine the impacts of faults on the crack initiation, failure pattern, and energy mechanism of the rock-like materials. Consequently, in this work, particle flow code is used to perform both experimental and numerical studies for rock-like material with edge notches, extending the prior experimental study (PFC2D). At the beginning, edge-notched gypsum sample experimental compressive tests are introduced. The gypsum micromechanical parameters are then calibrated using the results of earlier laboratory experiments. The PFC2D simulations are then run

for models with confined edges under uniaxial compression. The impact of the notch angle on the strength characteristics, deformation behaviors, and ultimate failure modes are then carefully assessed after having been simulated using PFC2D. Also the contrast between experimental testing and numerical modeling is made. The PFC2D findings can give valuable insight into the fracture propagation of rock pillars with edge faults in rock engineering.



Figure 1. Pillar with an edge connection [2].

2. Gypsum Pillar Tested under Uniaxial Compression with Two Edge Notches

Water and gypsum were at a 1.3 to 1 ratio. After 14 days of curing, Table 1 shows the tensile strength, compressive strength, Young modulus, and Poisson ratio. All of the experiments conducted in the current study were repeated three times to verify measurement accuracy, and the mean results are shown below. The trials employed gypsum materials to imitate a notched pillar. The components were combined to create the concoction. The specimen's measurements were set at 70 mm by 70 mm by 50 mm. Two plates were placed within the cubic mold to create the notched pillar, and after the sample had first hardened, they were taken out. Three test blocks with comparable prefabricated cracks were given for each set in order to improve test reliability and eliminate inadvertent mistakes. Two edge notches were included on every model. The angle of the 10 mm-long notch was 10, 20, and 30 degrees (Figure 2). The samples were kept for 14 days in dry, cold conditions. These samples were evaluated using a uniaxial machine with uniaxial compression (Figure 3). The loading speed was 0.05 mm/min.

Table 1. Gypsum's Young modulus, Poisson ratio, compressive strength, tensile strength, and other properties.

Strength in tension (MPa)	1.1
Strength in compression (MPa)	8
Modulus of Young (GPa)	5.5
Poisson ratio	0.27



(a)

(b)

(c)

Figure 2. Edge notched pillar with notch length of 10 mm and notch angle of a) 10°, b) 20°, and c) 30°.**Figure 3. Uniaxial loading frame.**

3. Test-failure Patterns in Laboratories

The failure process of samples with edge notches is shown in Figure 4. One significant splitting tensile fracture propagates across the model in all of the samples. Two wing fractures were initiated from the notch tips and progressed parallel to the loading axis until coalescence with the sample boundary when the notch angle was 10 (Figure 4a). One shear fracture started at the notch tip and spread diagonally across the rock bridge until coalescing with another notch tip when the notch angle was 20 (Figure 4b). When the notch angle was 30 degrees (Figure 4c), one wing fracture began at the left notch tip and spread parallel to the loading axis until coalescing with the sample boundary. Moreover, one shear fracture started at the apex of the notch and spread diagonally through the rock bridge before coalescing with the sample boundary.

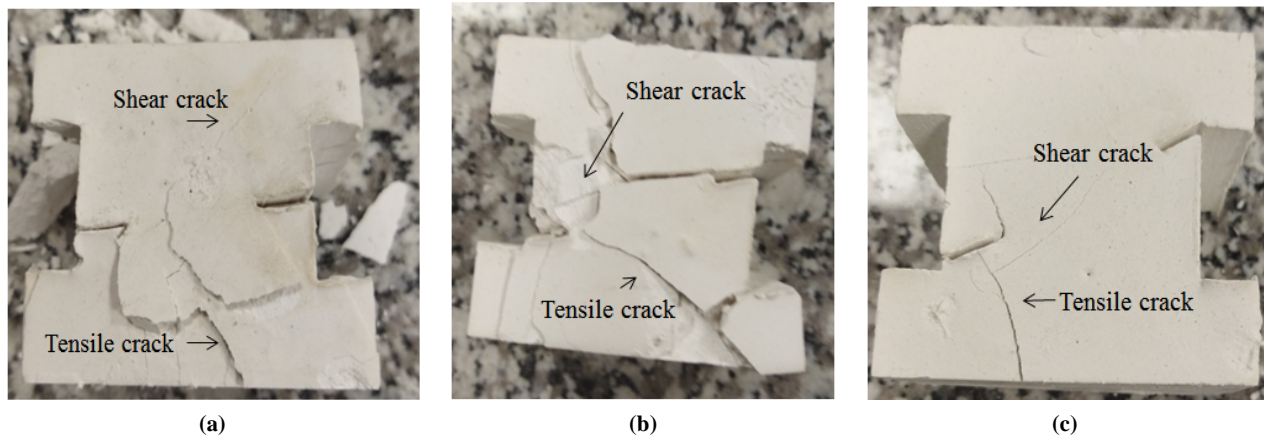


Figure 4. Failure pattern of physical samples containing edge notch with angle of a) 10°, b) 20°, and c) 30°.

4. Numerical Simulations

4.1. Particle flow code

The flat joint (FJ) model was put forth by Potyondy [33] by taking into account the hexagonal grain structure of the particles. The FJ contact is shown as a rigidly connected, locally smooth notional surface that is centered at the contact spot. Each component has a face, which serves as its hypothetical surface and communicates with other pieces' faces. As a result, each faced grain resembles a cylindrical or circular center with skirted faces. Lines or circles make up these features. Flat-jointed material is the name given to the collection of particles joined by FJ connections. The border between faced grains is divided into discrete components that may or may not be joined. The torque and force at each element are then reset to zero and updated in accordance with the force-displacement law of bond and the relative motion of faces after FJ has been inserted at a grain-to-grain contact. While the normal force is revised in a direct manner, the shear force is updated incrementally. The behavior of the bound element continues to be linear elastic as long as the strength does not go beyond its limit. By using flat joint model it is possible to calibrate the mechanical properties of numerical model according to experimental sample. Parallel bond or contact bond have limitation in this approach.

4.2. Preparation and testing of PFC2D model for rock-like substance

The typical procedure for creating a PFC2D assembly, which was completely detailed by Potyondy [33], was used to create a prototype model. Particle production, packaging, isotropic stress installation (stress initialization), drifting particle (floaters), removing, and bond installation make-up the procedure. The samples' weak gravitational effects make it possible for the gravitationally-induced tension gradient to have little impact on visible behavior. Utilizing Brazilian test and uniaxial compressive strength, the flat joint model and particle characteristics were calibrated [34]. A calibrated PFC particle assemblage was created using the micro-features and the accepted calibration techniques [34]. The porosity was chosen equal to 0.08 according to PFC manual to gain the standard particle number.

4.3. Numerical compression experiments on a granite pillar with cuts at edges

By building a box model in the PFC2D, uniaxial tests for rock pillar models were numerically simulated (Figure 5). The PFC samples have a 7 cm by 7 cm size. 1 cm wide was the pillar. 8231 disks with a minimum radius of 0.27 mm were included in the box sample. At the top and bottom of the model, there were two walls. The joint configurations are the same as the experimental ones, which is crucial to notice. Uniaxial forces were applied to the model via upper and lower walls. The model experienced an axial load rate of 0.05 mm/min. By measuring the response forces on the top wall, the compression force was calculated.

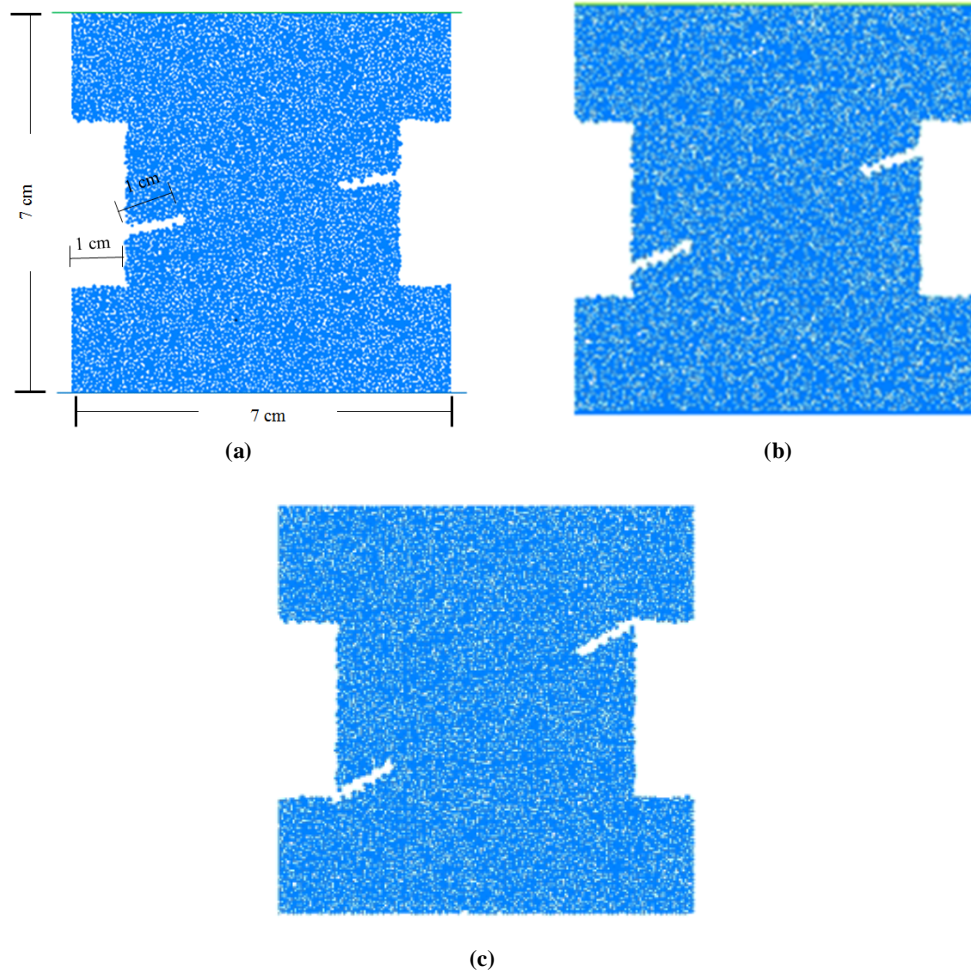


Figure 5. Edge notched pillar with notch length of 10 mm and notch angle of a) 10°, b) 20°, and c) 30°.

5. Failure Modes of Numerical Models

5.1. Pattern of failure

The failure mechanism of pillars with two edge notches is shown in Figure 6. Three different failure patterns were occurred in each model. In the first one, two tensile cracks started at the notch points and spread parallel to the loading axis until coalescing with the model boundary when the notch angle was 10°. In the second one, two tensile

cracks that started on the notch wall and coalesced with the pillar's left and right sides. There were two damaged areas on the model's two sides. In the third one, one splitting tensile crack developed through the model and leads major fracture. The same failure mechanism manifested itself at notch angles of 20° and 30°. It should be noted that by raising the notch angle, the damaged area's size grew.

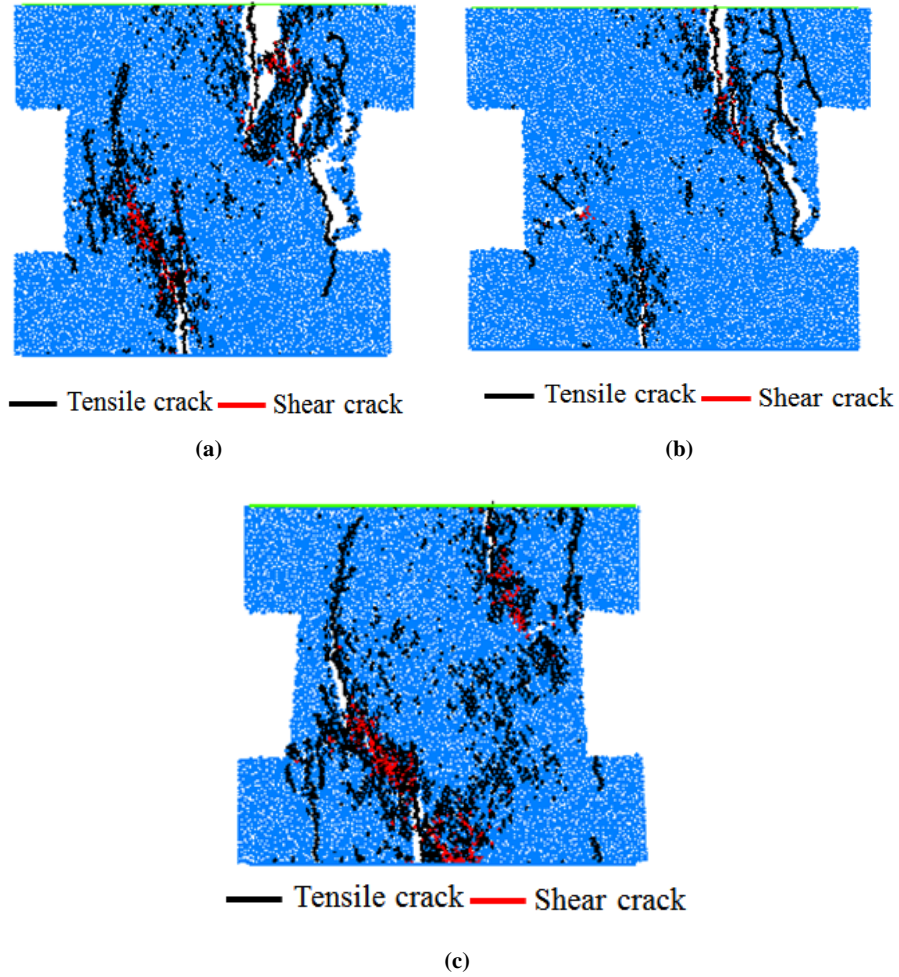


Figure 6. Failure pattern of models with notch angle of a) 10°, b) 20°, and c) 30°.

5.2. Ross diagram illustrating crack development

Ross diagrams of crack development in numerical models with various notch angles are shown in Figures 7a–c. The dip angle and the quantity of brand-new cracks are shown in the rose

diagram at the compression test's conclusion. The micro-crack angles in every model range from 75° to 105°. This indicates that the main fractures angle is unaffected by variations in the notch angle. When the notch angle reached 30°, the number of brand-new cracks peaked.

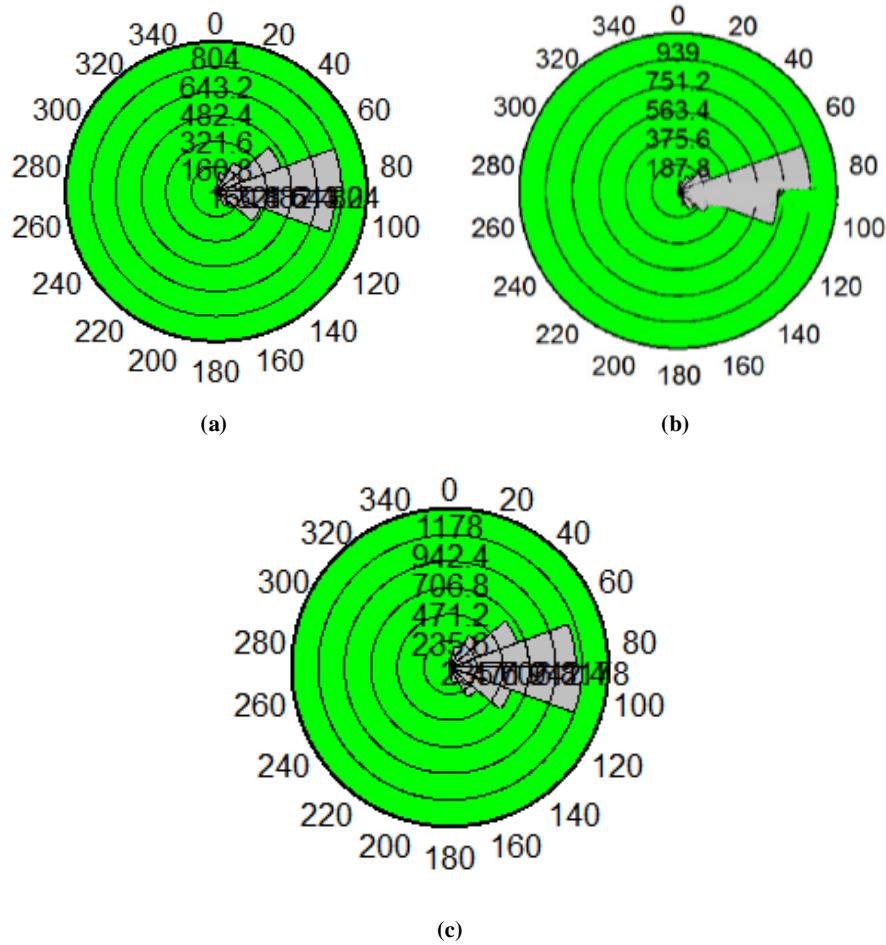


Figure 7. Ross diagram of crack growth in models with notch angle of a) 10°, b) 20°, and c) 30°.

5.3. Stress-strain graph with complete crack

The stress-strain curve along the overall fracture count is shown in Figure 8a–c for joints with 10, 20, and 30 degree angles, respectively. Five locations along the stress-strain curve, designated A to E, indicating 20, 40, 60, 80, and 100% of the total stress, respectively, were noted to verify at what stress level, the elastic range, the plastic range, and the ultimate failure happened. The calculated model's deformation reflected linear elastic performance, and the fracture frequency steadily increased. There were no fissures before point B, and raising the sample loading increases the number of cracks at stage BD. After the applied force achieved its maximum position and the fractures coalesced, the trajectory turned non-linear

and the rate of crack increment increased. Prior to the highest load, there is a small amount of variation brought on by the coalescence of significant fracture pairs. A rapid stress decrease occurs when the sample can no longer support the applied pressure, according to King *et al.* [35]. Because of the widespread macro-failure throughout the modeled sample, the stress decrease was greater after the highest load (point E). In actuality, more fractures occur when there is less stress decrease. Therefore, it can be assumed that each stress decrease during constant loading will cause the emergence of numerous fracture hits. It should be noted that raising the notch angle reduced the Young modulus of the models (dip angle of the linear portion of the stress-strain graph).

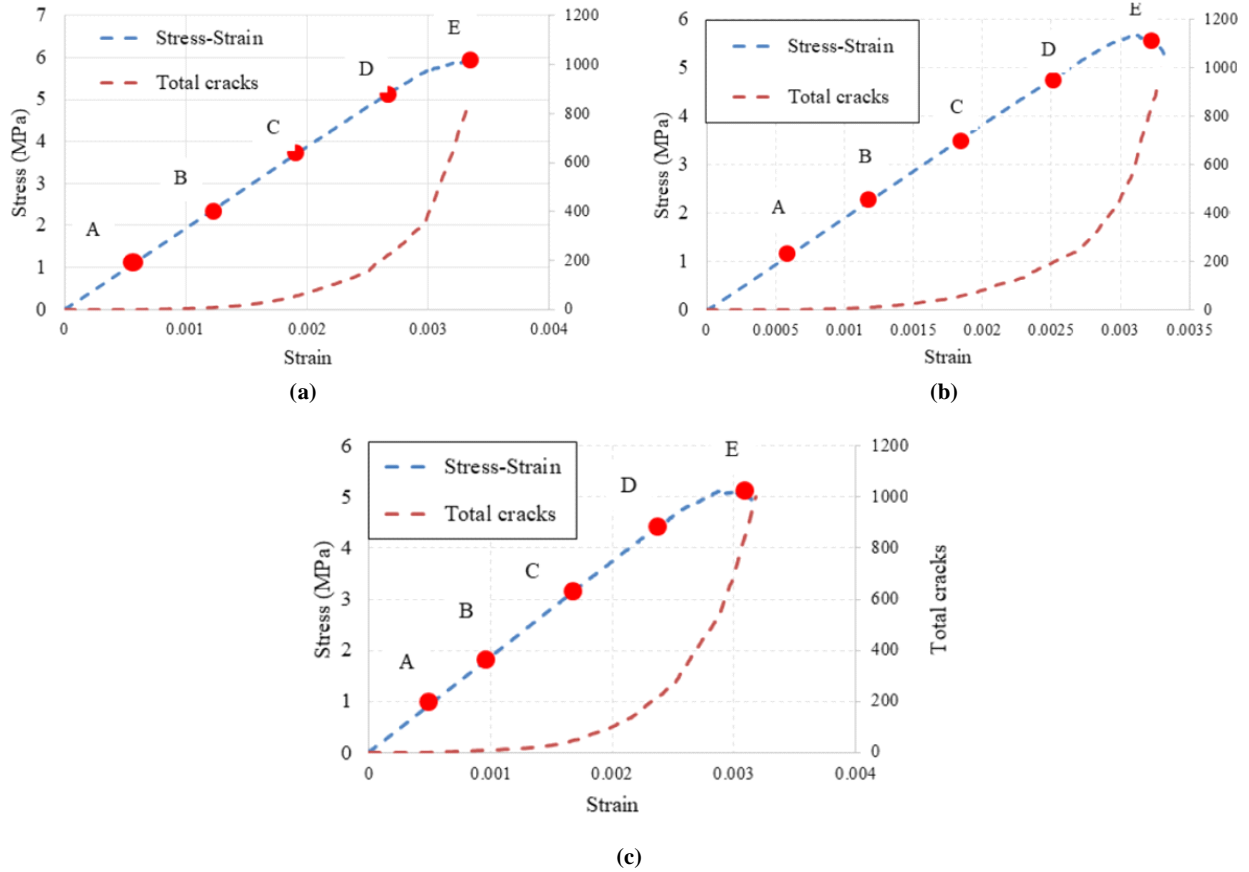


Figure 8. Stress–strain curve and cumulative crack number for notch angle of a)10°, b)20°, and c) 30°.

5.4. Effect of notch angle on model strength

The impact of notch angle on model strength is depicted in Figure 9. This image shows the outcomes of an experimental test and a numerical

calculation. The increase in slot angle resulted in a reduction in compressive strength. Both the experimental test and the numerical modeling showed a comparable tendency.

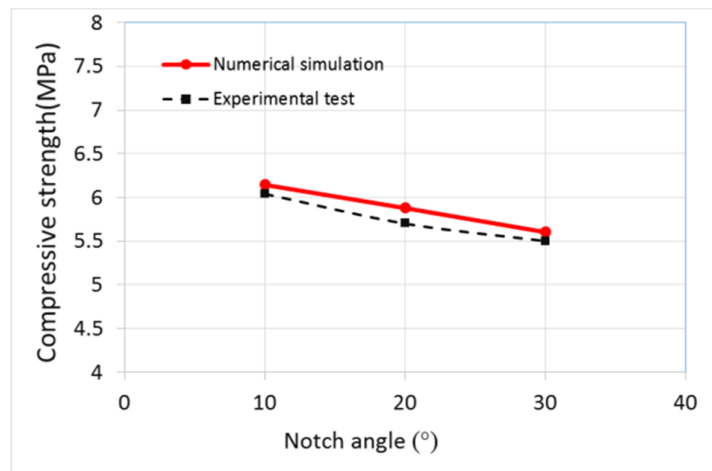


Figure 9. Effect of notch angle on model strength.

6. Conclusions

Investigating the failure behavior of rock pillars with various notch angles under uniaxial stress involved both experimental and discrete element techniques. Gypsum examples were created with dimensions of 70 mm * 70 mm * 50 mm. 10-, 20-, and 30-degree cut angles were used. The model received a horizontal force at a rate of 0.05 mm/min. The findings indicate that:

- In all models, two significant splitting tensile cracks started at the ends of the notches and progressed vertically until coalescing with the upper and lower model boundaries. On the left and right edges of the structure, two rock columns were also taken out.
- The angles of the micro-fractures ranged from 75° to 105° in all of the notch angles. This indicates that the main fractures angle is unaffected by variations in notch shape.
- Increasing the notch orientations resulted in a greater amount of newborn fractures.
- The overall number of fractures increased as sample loading grew. The model's deformation at the start of loading reflected linear elastic behavior, and the number of fractures steadily increased. When the number of cracks increased, the slope turned non-linear, and the force being applied peaked. When the sample can no longer resist the applied pressure, a rapid stress decrease occurs. The macro-failure throughout the entire model was what led to the greater stress decrease after the highest load. In actuality, the less stress decrease was accompanied by more overall fractures.
- By raising the notch angles, the compressive strength and Young modulus were both reduced.
- The experimental test and numerical simulation both show the same failure patterns.
- The numerical simulation and the experimental test, both display the same failure strengths.

References

[1]. Jaeger, J.C. and Cook N.G.W. (1979). *Fundamentals of Rock Mechanics*, 3rd Ed. NewYork, Chapman and Hall.

[2]. Esterhuizen, G.S. (2006). An evaluation of the strength of slender pillars. *Transactions of Society for Mining, Metallurgy, and Exploration, Inc.* Vol. 320. Littleton, CO: Society for Mining, Metallurgy, and Exploration, Inc, pp, 69–76.

[3]. Chiu, C.C. Weng, M.C. and Huang, T.H. (2016). Modeling rock joint behavior using a rough-joint model.

International Journal of Rock Mechanics and Mining Sciences, 89, 14-25

[4]. Hadjigeorgiou, J., Esmaili, K. and Grenon, M. (2009). Stability analysis of vertical excavations in hard rock by integrating a fracture system into a PFC model. *Tunneling and Underground Space Technology*, 24(3), 296-308

[5]. Qin, Z., Fu, H. and Chen, X.X. (2019). A study on altered granite meso-damage mechanisms due to water invasion-water loss cycles. *Environmental Earth Sciences*. 78 (14): 428, 1-10.

[6]. Wang, X. and Tian, L.G. (2018). Mechanical and crack evolution characteristics of coal-rock under different fracture-hole conditions: a numerical study based on particle flow code. *Environmental Earth Sciences*. 77 (8): 297, 1-10.

[7]. Wong, L.N.Y., Einstein, H.H. (2009). Crack coalescence in molded gypsum and carrara marble: part 1. macroscopic observations and interpretation. *Rock Mechanics and Rock Engineering*, 42, 475-511.

[8]. Zhou, X.P., Cheng, H. and Feng, Y.F. (2014). An experimental study of crack coalescence behavior in rock-like materials containing multiple flaws under uniaxial compression. *Rock Mechanics and Rock Engineering*, 47, 1961-1986

[9]. Shen, B., Stephansson, O., Einstein, H.H. and Ghahreman, B. (1995). Coalescence of fractures under shear stresses in experiments. *Journal of Geophysical Research*, 100, 5975-5990.

[10]. Mughieda, O. and Alzo'ubi, A.K. (2004). Fracture mechanisms of offset rock joints-a laboratory investigation. *Geotechnical and Geological Engineering*, 22, 545-562.

[11]. Cheng, Y., Wong, L. and Zou, C.J. (2015). Experimental study on the formation of faults from en - echelon fractures in carrara marble. *Engineering Geology*, 195,312-326.

[12]. Chiu, C.C., Weng, M.C., and Huang, T.H. (2016). Modeling rock joint behavior using a rough-joint model. *International Journal of Rock Mechanics and Mining Sciences*, 89, 14-25.

[13]. Zhang, B., Li, S.C., Zhou, F., Yang, X.Y., Xia, K.W., Liu, J.Y., Guo, S. and Wang, S.G. (2019). The coalescence and strength of rock-like materials containing two aligned X-type flaws under uniaxial compression. *Geomechanics and Engineering*, 17, 47-56.

[14]. Wang, X., Yuan, W., Yan, Y.T., and Zhang, X. (2020). Scale effect of mechanical properties of jointed rock mass: a numerical study based on particle flow code. *Geomechanics and Engineering*. 21 (3): 259-268.

[15]. Chai, S.B., Wang, H., Yu, L.Y., Shi, J.H. and Abi, E.D. (2020). Experimental Study on Static and Dynamic Compression Mechanical Properties of Filled Rock

Joints. Latin American Journal of Solids and Structures. 17 (3): 264.

[16]. Chen, C.S., Pan, E. and Amadei, B. (1998). Fracture mechanics analysis of cracked discs of anisotropic rock using the boundary element method. International Journal of Rock Mechanics and Mining Science. 35: 195-218.

[17]. Feng, X.T., Pan, P.Z. and Zhou, H. (2006). Simulation of the rock micro-fracturing process under uniaxial compression using an elasto-plastic cellular automaton. International Journal of Rock Mechanics and Mining Science, 43: 1091-1108.

[18]. Ning, Y., Yang, J., An, X. and Ma, G. (2011). Modelling rock fracturing and blast-induced rock mass failure via advanced discretisation within the discontinuous deformation analysis framework. Computers and Geotechnics. 38: 40-49.

[19]. Sarfarazi, V. and Haeri, H. (2022). PFC simulation of Brazilian tensile strength test in geomaterials' specimens with T-shaped non-persistent joints. Journal of Mining and Environment 13 (4): 1189-1209.

[20]. Potyondy, D.O. and Cundall, P.A. (2004). A bonded-particle model for rock. International Journal of Rock Mechanics and Mining Science, 41, 1329-1364.

[21]. Wu, Z.J. and Wong, L.N.Y. (2013). Elastic-plastic cracking analysis for brittle-ductile rocks using manifold method. International Journal of Fracture, 180, 71-91.

[22]. Yaylaci, M. and Birinci, A. (2013). The receding contact problem of two elastic layers supported by two elastic quarter planes. Structural Engineering and Mechanics. 48 (2): 241-255.

[23]. Yaylaci, M., Öner, E. and Birinci, A. (2014). Comparison between Analytical and ANSYS Calculations for a Receding contact Problem. Journal of Engineering Mechanics. 140 (9): 56-66.

[24]. Yaylaci, M. and Avcar, M. (2020). Finite element modeling of contact between an elastic layer and two elastic quarter planes. Computers and Concrete, Vol. 26, No. 2 (2020): 107-114.

[25]. Yaylaci, M., Terzi, C. and Avcar, M. (2019). Numerical analysis of the receding contact problem of two bonded layers resting on an elastic half plane. Structural Engineering and Mechanics. 72 (6).

[26]. Nehrii, S., Nehrii, T., Zolotarova, O. and Volkov, S. (2021). Investigation of the geomechanical state of soft adjoining rocks under protective constructions. Rudarsko-geološko-Naftni Zbornik (The Mining-Geological-Petroleum Bulletin). 36 (4): 61-71.

[27]. Nehrii, S., Nehrii, T., Kultaev, S. and Zolotarova, O. (2020). Providing resistance of protection means on the soft adjoining rocks. E3S Web Conf., 168, 00033. DOI: [10.1051/e3sconf/202016800033](https://doi.org/10.1051/e3sconf/202016800033).

[28]. Zhang, X.P. and Wong, L.N.Y. (2012). Cracking processes in rock-like material containing a single flaw under uniaxial compression: a numerical study based on parallel bonded-particle model approach. Rock Mechanics and Rock Engineering, 45, 711-737.

[29]. Fakhimi, A., Carvalho, F., Ishida, T. and Labuz, J.F. (2002). Simulation of failure around a circular opening in rock. International Journal of Rock Mechanics and Mining Science. 39: 507-515.

[30]. Lee, H. and Jeon, S. (2011). An experimental and numerical study of fracture coalescence in pre cracked specimens under uniaxial compression. International Journal of Solids and Structures. 48: 979-999.

[31]. Khazaei, C., Hazzard, J. and Chalaturnyk, R. (2015). Damage quantification of intact rocks using acoustic emission energies recorded during uniaxial compression test and discrete element modeling. Computers and Geotechnics. 67: 94-102.

[32]. Jin, J., Cao, P., Chen, Y., Pu, C.Z., Mao, D.W. and Fan, X. (2017). Influence of single flaw on the failure process and energy mechanics of rock-like material. Computers and Geotechnics. 86: 150-162.

[33]. Potyondy, D. O. (2015). The bonded-particle model as a tool for rock mechanics research and application: Current trends and future directions. Geosystem Engineering. 18 (1): 1-28.

[34]. Ghazvinian, A., Sarfarazi, V., Schubert, W. and Blumel, M. (2012). A study of the failure mechanism of planar non-persistent open joints using PFC2D. Rock Mechanics and Rock Engineering. 45 (5): 677-693.

[35]. King, M.S. and Pettitt, W.S. (2012). Young, Acoustic emissions associated with the formation of fracture sets in sandstone under polyaxial stress conditions Geophys. Prospect. 60 (2012): 93-102, <https://doi.org/10.1111/j.1365>.

مکانیزم شکست پایه سنگی حاوی دو درزه لبه‌ای؛ آزمون آزمایشگاهی و مدلسازی عددی

امیر رضایی، وهاب سرفرازی*، نیما بابانوری، محمد امیدی منش، و شیرین جهانمیری

بخش مهندسی معدن، دانشگاه صنعتی همدان، همدان، ایران

ارسال 2023/04/01، پذیرش 2023/04/18

* نویسنده مسئول مکاتبات: sarfarazi@hut.ac.ir

چکیده:

درزه‌های ناممتد بدلیل فعالیت‌های مختلف زمین‌شناسی در توده سنگ ایجاد می‌شوند که باعث کاهش مقاومت پایه‌های سنگی می‌گردند. در این مقاله، با استفاده از آزمون‌های آزمایشگاهی و مدلسازی عددی، نحوه رشد و گسترش ترک در پایه‌های سنگی حاوی درزه‌های ناممتد لبه‌ای مطالعه شده است. به این منظور پایه‌های گچ با ابعاد $70 \times 70 \times 50$ میلیمتر آماده سازی شد. مدول یانگ، نسبت پواسون، مقاومت فشاری و مقاومت کششی نمونه بکر برابر است با $5/5$ گیگاپاسکال، $0/27$ ، 8 مگاپاسکال و $1/1$ مگاپاسکال. دو درزه لبه‌ای ناممتد با زاویه‌های 10 درجه، 20 درجه و 30 درجه در پایه جایگذاری شده است. نمونه‌ها با نرخ بارگذاری $0/05$ میلیمتر بر دقیقه تحت آزمایش تک محوره قرار می‌گیرند. همزمان با انجام آزمون آزمایشگاهی، مدلسازی عددی روی مدل‌های پایه گچ انجام شد. نتایج نشان دادند که زاویه‌داری درزه تاثیر بسزایی بر الگوی شکست پایه دارد. الگوی شکست و مکانیزم شکست پایه توسط مقاومت پایه کنترل می‌شود. بدلیل تمرکز تنش در نوک درزه‌ها، دو ترک کششی از این نقاط شروع شده، بموازات محور بارگذاری رشد کرده و به لبه بالا و پایین نمونه متصل می‌شود. همچنین دو ترک کششی از دیواره درزه‌ها شروع شده، بطور مورب رشد کرده و به سمت چپ و راست پایه متصل می‌شود. به این ترتیب دو ستون سنگی از پایه جدا می‌شوند. در ابتدای بارگذاری رفتار مدل الاستیک است. با افزایش بارگذاری ترک‌های کمی در پایه و اطراف درزه شروع می‌شوند. نرخ ایجاد ترک‌ها ابتدا کم است ولی با افزایش بارگذاری تعداد ترک‌ها با نرخ زیادی افزایش می‌یابند و بطور ناپایدار رشد می‌کنند. در این مرحله منحنی تنش بر حسب کرنش رفتار غیر خطی دارد و سرانجام به نقطه تنش ماکزیمم می‌رسد. بعد از تنش ماکزیمم، منحنی تنش-کرنش افت می‌کند و رشد ناپایدار ترک افزایش می‌یابد. نتایج آزمایشگاهی و عددی در تطابق مناسب هستند.

کلمات کلیدی: پایه سنگی، درزه لبه‌ای، آزمون آزمایشگاهی، کد جریان ذره.